

A RECENT ACCRETION BURST IN THE LOW-MASS PROTOSTAR IRAS 15398–3359: ALMA IMAGING OF ITS RELATED CHEMISTRY

JES K. JØRGENSEN^{1,2}, RUUD VISSER³, NAMI SAKAI⁴, EDWIN A. BERGIN³, CHRISTIAN BRINCH^{1,2}, DANIEL HARSONO^{5,6},
JOHAN E. LINDBERG^{1,2}, EWINE F. VAN DISHOECK^{5,7}, SATOSHI YAMAMOTO⁴, SUZANNE E. BISSCHOP^{1,2}, AND MAGNUS V. PERSSON⁵

¹ Niels Bohr Institute, University of Copenhagen, Juliane Maries Vej 30, DK-2100 Copenhagen Ø., Denmark; jeskj@nbi.dk

² Centre for Star and Planet Formation and Natural History Museum of Denmark, University of Copenhagen, Øster Voldgade 5–7,
DK-1350 Copenhagen K., Denmark

³ Department of Astronomy, University of Michigan, 500 Church Street, Ann Arbor, MI 48109-1042, USA

⁴ Department of Physics, The University of Tokyo, 7-3-1 Hongo, Bunkyo-ku, Tokyo 113-0033, Japan

⁵ Leiden Observatory, Leiden University, P.O. Box 9513, NL-2300 RA Leiden, The Netherlands

⁶ SRON Netherlands Institute for Space Research, P.O. Box 800, 9700 AV, Groningen, The Netherlands

⁷ Max-Planck Institut für extraterrestrische Physik, Giessenbachstrasse, D-85748 Garching, Germany

Received 2013 October 21; accepted 2013 October 31; published 2013 December 4

ABSTRACT

Low-mass protostars have been suggested to show highly variable accretion rates throughout their evolution. Such changes in accretion, and related heating of their ambient envelopes, may trigger significant chemical variations on different spatial scales and from source-to-source. We present images of emission from $C^{17}O$, $H^{13}CO^+$, CH_3OH , $C^{34}S$ and C_2H toward the low-mass protostar IRAS 15398–3359 on $0''.5$ (75 AU diameter) scales with the Atacama Large Millimeter/submillimeter Array at 340 GHz. The resolved images show that the emission from $H^{13}CO^+$ is only present in a ring-like structure with a radius of about $1-1''.5$ (150–200 AU) whereas the CO and other high dipole moment molecules are centrally condensed toward the location of the central protostar. We propose that HCO^+ is destroyed by water vapor present on small scales. The origin of this water vapor is likely an accretion burst during the last 100–1000 yr increasing the luminosity of IRAS 15398–3359 by a factor of 100 above its current luminosity. Such a burst in luminosity can also explain the centrally condensed CH_3OH and extended warm carbon-chain chemistry observed in this source and furthermore be reflected in the relative faintness of its compact continuum emission compared to other protostars.

Key words: astrochemistry – ISM: abundances – ISM: individual objects (IRAS 15398-3359) – ISM: molecules – stars: formation – stars: protostars

Online-only material: color figures

1. INTRODUCTION

The discoveries of complex organic (and even prebiotic) molecules on small scales of low-mass protostars (Bottinelli et al. 2004; Jørgensen et al. 2005, 2012) as well as the presence of rotationally supported disks relatively early in their evolution (Tobin et al. 2012; Murillo et al. 2013; Lindberg et al. 2013) sets an interesting frame for the question: what are the initial conditions for the chemistry in young solar system analogs? One of the key challenges is to follow the chemistry with increasing temperature and density as material falls in from molecular clouds to solar system scales close to the young star.

The chemistry leading to the formation of larger molecules likely involves a complex balance between molecules freezing out on dust grains, grain surface chemistry and eventual evaporation of the species before they may be (re-)incorporated in ices in the circumstellar disks (see, e.g., Herbst & van Dishoeck 2009; Caselli & Ceccarelli 2012, for recent reviews). However, not only does this depend on the wide-ranging network of chemical reactions—but more fundamentally also on the exact physical history of material as it is accreted. In the simplest picture the temperature increases monotonically as material falls in closer to the central protostar at a constant rate. In reality, however, variations in, for example, the accretion rate may strongly affect the protostellar luminosity and thus temperature throughout the cloud. Since the dust temperature is crucial for the gas-grain chemistry, luminosity variations can have a strong effect on the radial distribution of the chemistry—and from source to source.

With the high angular resolution and surface brightness sensitivity of the Atacama Large Millimeter/submillimeter

Array (ALMA), it is becoming possible to image the distribution of molecular species toward individual protostars on solar system scales. This paper presents ALMA images of the deeply embedded protostar IRAS 15398–3359 (hereafter IRAS 15398), located in the Lupus I molecular cloud (B228) (Heyer & Graham 1989; Chapman et al. 2007) at a distance of 155 pc (Lombardi et al. 2008). From a reanalysis of its spectral energy distribution (SED) and submillimeter continuum maps, its luminosity $L_{bol} = 1.8 L_{\odot}$, bolometric temperature, $T_{bol} = 44$ K and envelope mass, $M_{env} \approx 1.2 M_{\odot}$ makes it a fairly standard “Class 0” low-mass protostar. From a chemical point of view IRAS 15398 is interesting as it is one of two prototypical sources with prominent carbon-chain molecules such as C_4H , C_4H_2 , CH_3CCH and HC_5N (Sakai et al. 2009). This peculiar chemistry has been suggested to be either an indication of the primordial conditions of the clouds and relative time-scales and degrees of freeze-out for CO and CH_4 (Sakai et al. 2009) or a flatter density and temperature profile on larger scales of the envelope (e.g., Herbst & van Dishoeck 2009). The main aim of this paper is to relate the observed chemical emission signatures to the physical structure and evolution of the protostar.

2. OBSERVATIONS

IRAS 15398–3359 was observed on four occasions between 2012 March 29 and 2012 April 11 as part of the ALMA Early Science Cycle 0 program 2011.0.00628.S (PI Jes Jørgensen) at 0.87 mm (ALMA band 7). At the time of observations 15–16 antennae were present in the array in an extended configuration providing baselines ranging from

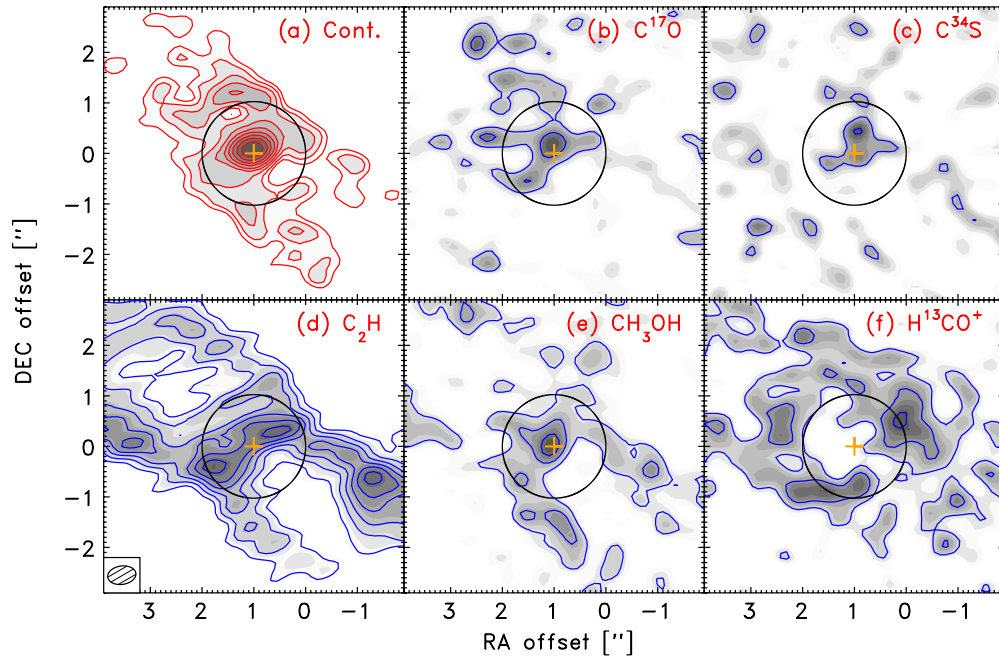


Figure 1. Maps of the continuum (a) and integrated line emission toward IRAS15398 for (b) C^{17}O $J = 3-2$, (c) C^{34}S $J = 7-6$, (d) C_2H $N = 4-3$, $J = 7/2-5/2$, (e) CH_3OH $J_k = 7_0-6_0$, and (f) H^{13}CO^+ $J = 4-3$. For the continuum the contours are given in 10 logarithmic steps from 4σ ($0.8 \text{ mJy beam}^{-1}$) to the maximum (19 mJy beam^{-1}). For each line, the emission is integrated over velocity intervals of $\pm 1 \text{ km s}^{-1}$ from systemic velocity—except for C_2H , which is integrated over $\pm 1.5 \text{ km s}^{-1}$ around 349.40 GHz to cover the two, $F = 4-3$ and $F = 3-2$, transitions of that species. The emission contours are shown in steps of 3σ ($1\sigma \approx 5 \text{ mJy beam}^{-1} \text{ km s}^{-1}$).

(A color version of this figure is available in the online journal.)

20–392 m ($\approx 23\text{--}445 \text{ k}\lambda$). The phase center was taken to be $\alpha = 15^{\text{h}}43^{\text{m}}02^{\text{s}}.16$; $\delta = -34^{\circ}09'06''.80$ [J2000]. Over the four observing sessions IRAS15398 was observed with a total on-source integration time of about three hours.

The observations contain four spectral windows with 3840 channels and a channel width of 122 kHz (0.11 km s^{-1}). The spectral setup was chosen to cover 336.95–337.45 GHz, 338.30–338.80 GHz, 349.35–349.85 GHz and 346.90–347.40 GHz. A second dataset obtained in connection with this program, targeting the protostar R CrA-IRS7B with a similar spectral setup, is presented by Lindberg et al. (2013).

The reduction followed standard recipes in CASA⁸ (McMullin et al. 2007) with calibration of the complex gains through observations of the quasar J1517-243, passband calibration on J1325-430 and flux calibration on Neptune and Titan. This procedure provides a dataset with a beam size of about $0''.55 \times 0''.37$ (P.A. = -82°), slightly varying with wavelength, and an rms level of $13 \text{ mJy beam}^{-1} \text{ channel}^{-1}$. The continuum was constructed by averaging the channels across the four spectral bands that appear reasonably free of line emission with a resulting rms level of about $0.28 \text{ mJy beam}^{-1}$.

The CH_3OH $7_k - 6_k$ transitions at 338.3–338.7 GHz were also targeted in a parallel program (2011.0.00777.S; PI Nami Sakai) and observed with 24 antennas for 1 hr on-source. For those CH_3OH transitions as well as the continuum we combine the datasets for a slight improvement in signal-to-noise.

3. RESULTS

The continuum emission from IRAS15398 is clearly detected at $\alpha = 15^{\text{h}}43^{\text{m}}02^{\text{s}}.24$; $\delta = -34^{\circ}09'06''.71$ [J2000] with a peak flux of 19 mJy beam^{-1} and integrated flux of 28 mJy (Figure 1(a)).

For comparison the JCMT/SCUBA image of IRAS15398 from the SCUBA legacy archive (Di Francesco et al. 2008) shows the core on larger scales with a total integrated flux of 3.9 Jy at $850 \mu\text{m}$. The bright part of the continuum emission in the ALMA maps is largely unresolved. Some low level extended emission is seen though, reflecting the resolved-out low surface brightness emission from the ambient envelope seen in the James Clerk Maxwell Telescope (JCMT) data. Generally, emission that is smooth on scales much larger than $9''$ (1400 AU) or present on scales larger than $16''$ (2500 AU) will be unreliable due to the lack of short baselines and size of the ALMA primary beam at 345 GHz.

Figures 1 and 2 show images and spectra for the detected lines while Figure 3 includes a full overview of the four spectral settings. Toward the continuum position, transitions of five different species are detected: C^{17}O $J = 3-2$, C^{34}S $J = 7-6$, C_2H $N = 4-3$, $J = 7/2-5/2$, H^{13}CO^+ $J = 4-3$ and a range of the CH_3OH $J_k = 7_k - 6_k$ transitions at 338 GHz. In addition, there are a few lines that tentatively can be assigned to CH_3CN and CH_3OH at 349.4–349.7 GHz. The most noteworthy non-detection is SiO 8–7 suggesting that there is no strong shock activity on small scales. The line-profiles are relatively narrow (FWHM $\approx 0.5\text{--}0.7 \text{ km s}^{-1}$) and symmetric. All lines are detected at a systemic velocity of 5.0 km s^{-1} with the exception of H^{13}CO^+ 4–3 that peaks red-shifted by about 1.0 km s^{-1} compared to the other species. The C^{17}O , C^{34}S and CH_3OH emission is found toward the central continuum peak and concentrated within about one arcsecond radius (Figure 1). H^{13}CO^+ in contrast is predominantly present beyond this radius in a ring-like structure with a width of about $1''$. A more detailed discussion of the extended C_2H emission related to the outflow is deferred to a separate publication (Y. Oya et al., in preparation). The detection of CH_3OH and tentative detections of CH_3CN and

⁸ <http://casa.nrao.edu/>

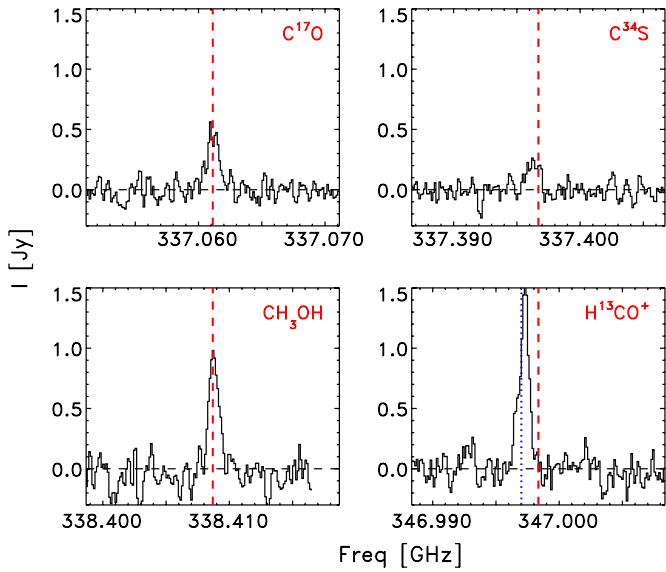


Figure 2. Spectra of $C^{17}O$ 3–2, $C^{34}S$ 7–6, CH_3OH 7₀–6₀, and $H^{13}CO^+$ 4–3 obtained by integration over the inner 2'' (radius) toward the continuum peak of IRAS15398. Each spectrum has been corrected by a systemic velocity of 5.0 km s⁻¹. In each panel the vertical dashed (red) lines indicates the rest frequency of the given transition. In the $H^{13}CO^+$ panel, the dotted line indicates the frequency corresponding to a systemic velocity of 6.0 km s⁻¹.

(A color version of this figure is available in the online journal.)

CH_3OCH_3 mark the first discoveries of these complex organic species toward one of the sources characterized by the presence of carbon-chain molecules.

The velocity offset and peculiar morphology of $H^{13}CO^+$ is significant. The $H^{13}CO^+$ line profile itself is very symmetric and no emission or absorption is seen at the lower LSR velocity of the other species. Together with the extended continuum and C_2H emission being present on-source and the lack of clear negative bowls of emission, this suggests that spatial-filtering or limited dynamical range due to the (u, v) -coverage is not the reason. Instead it suggests that $H^{13}CO^+$ is present in gas that is kinematically and morphologically different than the other species. With the current sensitivity and resolution it is not possible to address the kinematic nature of this component further, however.

4. DISCUSSION

The most striking aspect of the data is the presence of $C^{17}O$ and lack of $H^{13}CO^+$ toward the central position in IRAS15398. An explanation could be that the innermost region represents a lower density environment where $C^{17}O$ 3–2 could be excited and not the higher density tracer $H^{13}CO^+$ 4–3. However, with the additional detections of $C^{34}S$ and CH_3OH on small scales this can be ruled out. The differences between these species must be the result of their chemistry.

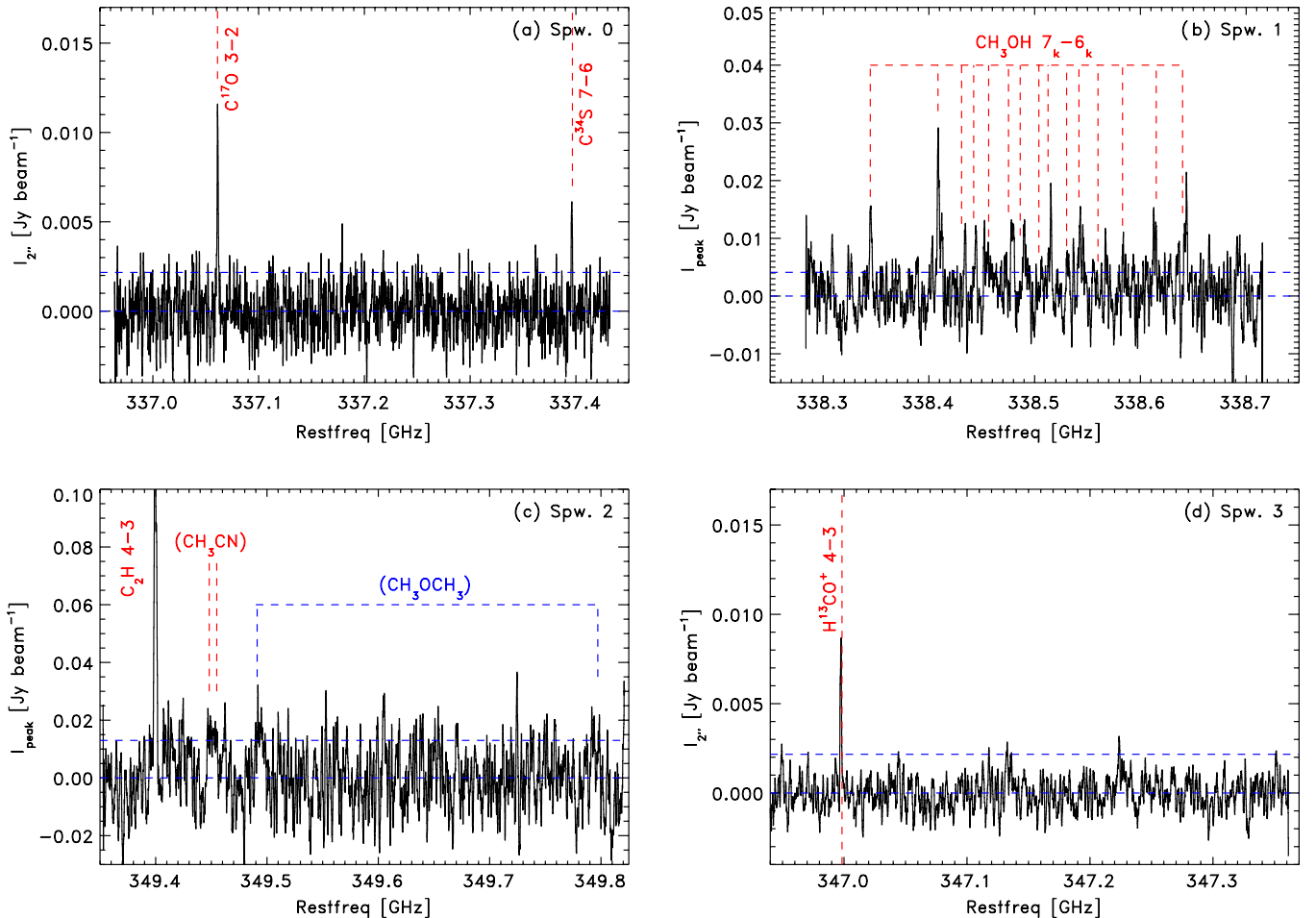


Figure 3. Spectra from the four covered spectral windows taken in the central pixel toward the continuum peak (panels (b) and (c)) or averaged over the inner 2'' region (panels (a) and (d)). In panel (b) all cataloged CH_3OH 7_k – 6_k transitions have been marked—no matter whether they were detected or not.

(A color version of this figure is available in the online journal.)

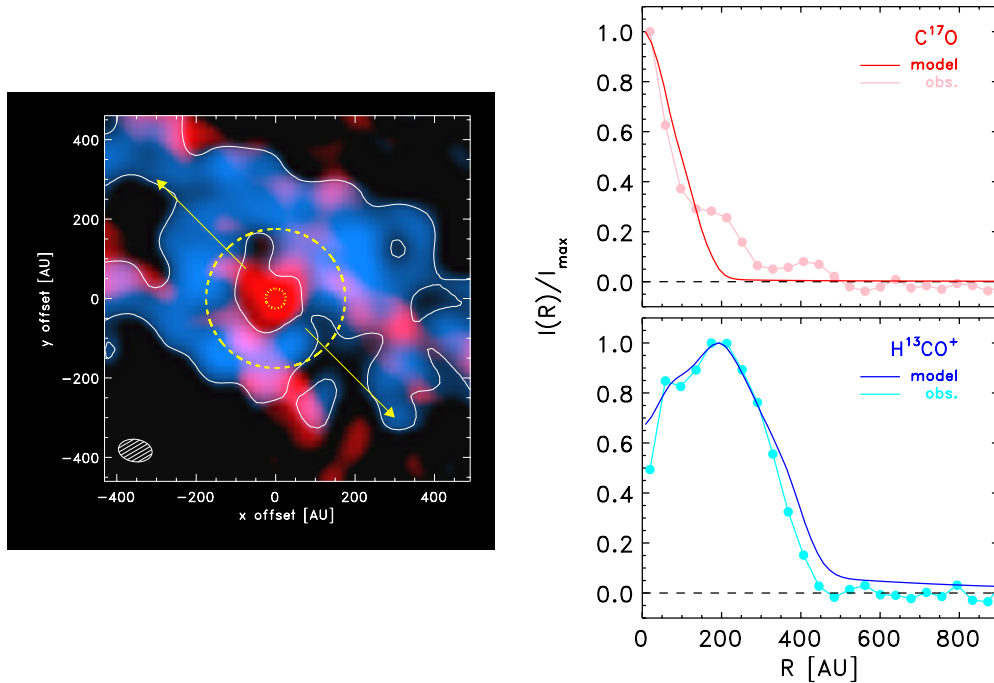
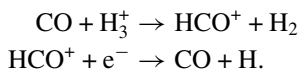


Figure 4. Left: observed emission of CH_3OH (red) and H^{13}CO^+ (blue) compared to the physical scales of the source and with the observed beam is shown in the bottom left corner. The dotted and dashed circles indicate the radii where the temperature has dropped to 100 K and 30 K, respectively, according to the dust radiative transfer model for the envelope. The arrows indicate the propagation direction of the IRAS15398 outflow. Right: observed radial profiles of C^{17}O 3–2 and H^{13}CO^+ 4–3 compared to radiative transfer models of both species. For C^{17}O the abundance changes from 5×10^{-8} (a CO abundance of 1×10^{-4}) in the inner regions of the envelope to 5×10^{-10} at the radius where the temperature drops below 30 K (i.e., depletion by a factor 100). For H^{13}CO^+ the abundance is 7×10^{-11} in the region of the envelope where the temperature is between 20 K and 30 K. Inside and outside this region the H^{13}CO^+ abundance must be at least a factor 20 lower. (A color version of this figure is available in the online journal.)

At the densities and temperatures of the bulk protostellar envelope material, the abundances of CO and HCO^+ are related through the main formation and destruction mechanisms for HCO^+ :



Indeed, over large ranges of CO abundances seen in protostars, these two species are observed to be strongly correlated, likely to first order reflecting the chemistry driven by the freeze-out of CO (Jørgensen et al. 2004b). The anti-correlation between CO and HCO^+ in our images suggests that another process is at work as well.

The observed profiles of C^{17}O and H^{13}CO^+ can be used to quantify their abundances through line radiative transfer modeling. For this purpose, we adopted a one-dimensional model for the IRAS15398 envelope with a power-law density profile, constrained by the SED and submillimeter continuum images, and with the temperature distribution calculated self-consistently using the Transphere code⁹ (Dullemond et al. 2002). The IRAS15398 envelope is well-fit with a power-law density profile decreasing toward larger radii as $n(\text{H}_2) \propto r^{-p}$ with $p = 1.5\text{--}2$ and a density of $(1\text{--}3) \times 10^7 \text{ cm}^{-3}$ and a temperature of 30 K at 175–200 AU (1–1/5).

Subsequently the line radiative transfer was performed for C^{17}O and H^{13}CO^+ using the one-dimensional RATRAN code (Hogerheijde & van der Tak 2000) following the same approach as in, e.g., Jørgensen (2004): the abundances of the two species

were taken to be constant in regions separated at specific temperatures and adjusted to match the observed brightness profiles (Figure 4). It is possible to reproduce the observed emission for C^{17}O with an abundance of 5×10^{-8} (a CO abundance of 1×10^{-4}) in the inner regions of the envelope with temperatures above 30 K (175 AU) and 5×10^{-10} at larger radii (i.e., depletion by a factor 100). This confirms the expectation that C^{17}O is present in the inner regions of the envelopes where the temperature increases above the CO sublimation temperature—similar to what is seen in other protostars (e.g., Jørgensen 2004). For H^{13}CO^+ , in contrast, it is only possible to reproduce the observed profiles with an abundance of 7×10^{-11} (HCO^+ abundance of 5×10^{-9}) in the region of the envelope where the temperature is between 20 K and 30 K and a drop in abundance of at least a factor 20 inside and outside this region.

A possible explanation for the depletion of HCO^+ on small scales is that it is destroyed by dipolar, neutral molecules. The most abundant of these is H_2O , which is predominantly present in a solid form in protostellar envelopes. However, in regions where the temperatures increase above 100 K, water sublimates and becomes an important destroyer of HCO^+ . Figure 5 shows the result of a steady state calculation based on the more detailed models of Visser & Bergin (2012) utilizing the UDA12 gas-phase chemical network (McElroy et al. 2013). In this simple calculation we show the HCO^+ abundance as function of H_2O and C_2H abundance at a density of 10^7 cm^{-3} , temperature of 30 K and cosmic ray ionization rate of $5 \times 10^{17} \text{ s}^{-1}$. An H_2O abundance increase to 10^{-6} is enough to reduce HCO^+ by two orders of magnitude—matching the inferred abundance profile inferred from the observations. Alternatively, other neutral species, such as the carbon-chain molecules or H_2CO , could also work as destroyers of HCO^+ . However, due to their weaker

⁹ <http://www.ita.uni-heidelberg.de/~dullemond/software/transphere/index.shtml>

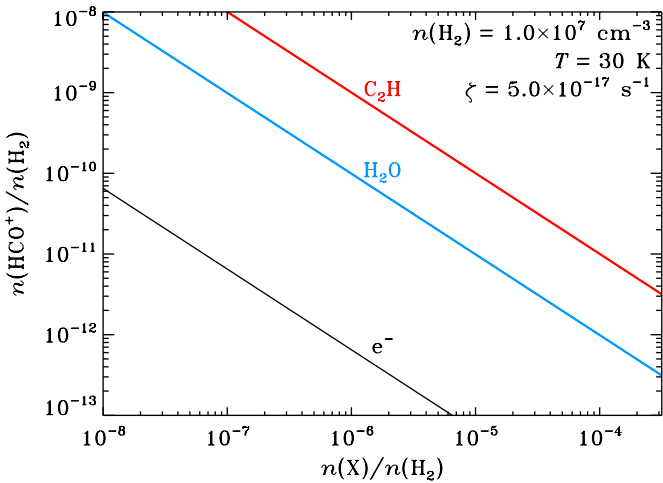


Figure 5. Abundance of HCO^+ as function of H_2O (blue) and C_2H (red) abundance in a gas with a density of 10^7 cm^{-3} and a temperature of 30 K in a chemical model based on Visser & Bergin (2012). For water abundances as low as 10^{-6} , the HCO^+ abundance is reduced by two orders of magnitude to the observed $\sim 10^{-10}$. Similar levels of destruction by C_2H require an abundance of that species an order of magnitude larger, about 10^{-5} .

(A color version of this figure is available in the online journal.)

dipole moments, their abundances need to be comparably larger to destroy HCO^+ efficiently (Figure 5). For example, in the chemical models by Aikawa et al. (2012), H_2CO is the main destroyer of HCO^+ at intermediate temperatures—but the gas-phase abundances of H_2CO in those models are as high as 10^{-5} , which are not supported by observations of low-mass protostars that show typical abundances of $\text{H}_2\text{CO} \lesssim 10^{-7}$ in the warm gas (e.g., Ceccarelli et al. 2000; Schöier et al. 2002, 2004).

The main issue regarding the scenario in which water acts as the main destroyer is that temperatures of 100 K are only reached in the inner 25 AU for a $1.8 L_\odot$ source such as IRAS15398—much smaller than the H^{13}CO^+ ring. High water abundances on large scales could be caused by, e.g., an outflow-driven shock—and indeed lead to the destruction of HCO^+ (e.g., Bergin et al. 1998; Jørgensen et al. 2004a). Water is detected toward IRAS15398 with Herschel-PACS and found to be associated with the outflow (Karska et al. 2013), but the ring-like structure of H^{13}CO^+ and relatively narrow lines of CH_3OH (another molecule that could be produced by ice sputtering) speak against this being the reason for the observed emission structures here. Another solution is that IRAS15398 has recently undergone a change in luminosity, e.g., related to a burst in accretion. Such accretion bursts have been proposed to be characteristic of embedded protostellar stages and invoked to explain, for example, the distribution of observed luminosities of embedded protostars (e.g., Kenyon et al. 1990; Vorobyov & Basu 2006; Evans et al. 2009; Dunham & Vorobyov 2012). An increase in luminosity would sublimate water in a much larger region than hinted at by its current luminosity and after the burst water would stay in the gas-phase for a period of time corresponding to the H_2O freeze-out time-scales. To sublimate water at a distance of 175 AU of IRAS15398, its luminosity (and accretion rate) should have been higher by two orders of magnitude than currently. At the density of the IRAS15398 envelope at this distance of 10^7 cm^{-3} , the time-scale for water to freeze-out is of order 100–1000 yr, which can be considered to be an upper limit to the time since the burst.

Unfortunately no direct imaging of the water vapor in IRAS15398 exists, but CH_3OH may work as a good proxy for

water as it desorbs at similar temperatures. Figure 3 illustrates that CH_3OH is indeed present and extended on the scales where H^{13}CO^+ is absent, lending further credibility to this suggestion. A simple estimate using *Radex* (van der Tak et al. 2007) shows that the C^{17}O 3–2 and CH_3OH 7_0-6_0 are similar in strength for a $[\text{CH}_3\text{OH}]/[\text{CO}]$ abundance ratio of 6×10^{-5} at the density of 10^7 cm^{-3} and temperature of 30 K characteristic of the CH_3OH emitting region. Assuming a standard CO abundance of $\sim 10^{-4}$, this translates into a CH_3OH abundance with respect to H_2 of $\sim 10^{-8}$ in this inner region.

The suggestion of a recent episodic accretion burst also raises another interesting perspective, namely it may have triggered the chemistry leading to the formation of warm carbon-chain molecules on large scales in the IRAS15398 envelope. Observations of the two prototypical sources, L1527 and IRAS15398, show that these carbon-chain molecules are present on large scales of a few thousand AU but with a sharp abundance increase inward of 1000 AU (Sakai et al. 2008, 2009). Sakai et al. mentioned that the widespread emission is related to carbon-chain molecules produced in the early phase of prestellar evolution, but the additional increase at 1000 AU scales requires that CH_4 is present in the gas-phase at temperatures of ≈ 30 K (see also Hassel et al. 2008). From the model above, the envelope temperatures of IRAS15398 is currently only about 15 K on the 1000 AU scales and only reach 30 K in the inner 175 AU. However, if it has undergone a burst in recent history this could have caused CH_4 to evaporate and trigger the carbon-chain chemistry at much larger radii: an increase in luminosity by a factor 50–100 would for example shift the radius where the temperature is 30 K out to 1500–2200 AU.

It is interesting to note that L1527 and IRAS15398 both contain relatively weak compact continuum emission compared to many other deeply embedded protostars (e.g., Jørgensen et al. 2009). With the assumption in that paper, the observed compact continuum emission on baselines $\gtrsim 50 \text{ k}\lambda$ corresponds to $0.029 M_\odot$ in L1527 and $<0.01 M_\odot$ in IRAS15398—compared to the median $0.089 M_\odot$ for the Class 0 protostars. The nature of this compact continuum emission is still unclear—but one possibility is that it reflects the build-up of an unstable (pseudo-)disk (Jørgensen et al. 2009). In that scenario, the absence of strong compact continuum emission toward these two sources would indicate that they have recently shedded these massive disks.

In summary, the proposed scenario of a recent accretion burst explains four characteristic signatures observed toward IRAS15398: (1) the clear absence of HCO^+ in the region with prominent CO emission, (2) the presence of extended CH_3OH emission relative to its current luminosity, (3) the presence of warm carbon-chain molecules on large scales and (4) the absence of a very massive dust continuum component on small scales. Although different mechanisms can possibly explain any one of these signatures, the strength of the proposed scenario is that it accounts for all. If the scenario is confirmed through similar observations of other protostars, statistics of the detections of such signatures could shed further light onto the frequency of similar bursts during the embedded protostellar stages.

We thank the referee, Andrew Walsh, for a prompt and constructive report. This paper makes use of ALMA dataset ADS/JAO.ALMA#2011.0.00628.S. ALMA is a partnership of ESO (representing its member states), NSF (USA) and NIN S (Japan), together with NRC (Canada) and NSC and ASIAA (Taiwan), in cooperation with the Republic of

Chile. The Joint ALMA Observatory is operated by ESO, AUI/NRAO and NAOJ. This research was supported by a Lundbeck Foundation Junior Group Leader Fellowship to Jes Jørgensen. Centre for Star and Planet Formation is funded by the Danish National Research Foundation. We also acknowledge support from National Science Foundation grant 1008800 and EU A-ERC grant 291141 CHEMPLAN.

REFERENCES

- Aikawa, Y., Wakelam, V., Hersant, F., Garrod, R. T., & Herbst, E. 2012, *ApJ*, **760**, 40
- Bergin, E. A., Neufeld, D. A., & Melnick, G. J. 1998, *ApJ*, **499**, 777
- Bottinelli, S., Ceccarelli, C., Neri, R., et al. 2004, *ApJL*, **617**, L69
- Caselli, P., & Ceccarelli, C. 2012, *A&ARv*, **20**, 56
- Ceccarelli, C., Loinard, L., Castets, A., Tielens, A. G. G. M., & Caux, E. 2000, *A&A*, **357**, L9
- Chapman, N. L., Lai, S.-P., Mundy, L. G., et al. 2007, *ApJ*, **667**, 288
- Di Francesco, J., Johnstone, D., Kirk, H., MacKenzie, T., & Ledwosinska, E. 2008, *ApJS*, **175**, 277
- Dullemond, C. P., van Zadelhoff, G. J., & Natta, A. 2002, *A&A*, **389**, 464
- Dunham, M. M., & Vorobyov, E. I. 2012, *ApJ*, **747**, 52
- Evans, N. J., Dunham, M. M., Jørgensen, J. K., et al. 2009, *ApJS*, **181**, 321
- Hassel, G. E., Herbst, E., & Garrod, R. T. 2008, *ApJ*, **681**, 1385
- Herbst, E., & van Dishoeck, E. F. 2009, *ARA&A*, **47**, 427
- Heyer, M. H., & Graham, J. A. 1989, *PASP*, **101**, 816
- Hogerheijde, M. R., & van der Tak, F. F. S. 2000, *A&A*, **362**, 697
- Jørgensen, J. K. 2004, *A&A*, **424**, 589
- Jørgensen, J. K., Bourke, T. L., Myers, P. C., et al. 2005, *ApJ*, **632**, 973
- Jørgensen, J. K., Favre, C., Bisschop, S. E., et al. 2012, *ApJL*, **757**, L4
- Jørgensen, J. K., Hogerheijde, M. R., Blake, G. A., et al. 2004a, *A&A*, **415**, 1021
- Jørgensen, J. K., Schöier, F. L., & van Dishoeck, E. F. 2004b, *A&A*, **416**, 603
- Jørgensen, J. K., van Dishoeck, E. F., Visser, R., et al. 2009, *A&A*, **507**, 861
- Karska, A., Herczeg, G. J., van Dishoeck, E. F., et al. 2013, *A&A*, **552**, A141
- Kenyon, S. J., Hartmann, L. W., Strom, K. M., & Strom, S. E. 1990, *AJ*, **99**, 869
- Lindberg, J. E., Jørgensen, J. K., Brinch, C., et al. 2013, *A&A*, submitted
- Lombardi, M., Lada, C. J., & Alves, J. 2008, *A&A*, **480**, 785
- McElroy, D., Walsh, C., Markwick, A. J., et al. 2013, *A&A*, **550**, A36
- McMullin, J. P., Waters, B., Schiebel, D., Young, W., & Golap, K. 2007, in ASP Conf. Ser. 376, *Astronomical Data Analysis Software and Systems XVI*, ed. R. A. Shaw, F. Hill, & D. J. Bell, 127
- Murillo, N. M., Lai, S. P., Bruderer, S., Harsono, D., & van Dishoeck, E. F. 2013, *A&A*, in press (arXiv:1310.8481)
- Sakai, N., Sakai, T., Hirota, T., Burton, M., & Yamamoto, S. 2009, *ApJ*, **697**, 769
- Sakai, N., Sakai, T., Hirota, T., & Yamamoto, S. 2008, *ApJ*, **672**, 371
- Schöier, F. L., Jørgensen, J. K., van Dishoeck, E. F., & Blake, G. A. 2002, *A&A*, **390**, 1001
- Schöier, F. L., Jørgensen, J. K., van Dishoeck, E. F., & Blake, G. A. 2004, *A&A*, **418**, 185
- Tobin, J. J., Hartmann, L., Chiang, H.-F., et al. 2012, *Natur*, **492**, 83
- van der Tak, F. F. S., Black, J. H., Schöier, F. L., Jansen, D. J., & van Dishoeck, E. F. 2007, *A&A*, **468**, 627
- Visser, R., & Bergin, E. A. 2012, *ApJL*, **754**, L18
- Vorobyov, E. I., & Basu, S. 2006, *ApJ*, **650**, 956